FISEVIER

Contents lists available at ScienceDirect

Journal of Molecular Spectroscopy

journal homepage: www.elsevier.com/locate/jms



Perturbations of the $A^{\prime 1}\Pi$ and $C^{1}\Sigma^{+}$ states of CaO

Sean M. Bresler^a, Joel R. Schmitz^a, Michael C. Heaven^{a,*}, Robert W. Field^b



^b Department of Chemistry, Massachusetts Institute of Technology, Cambridge, MA 02139, United States



ARTICLE INFO

Article history: Received 10 March 2020 In revised form 13 April 2020 Accepted 15 April 2020 Available online 22 April 2020

Keywords: CaO Electronic spectroscopy Perturbations Electronic structure

ABSTRACT

Laser induced fluorescence spectra for jet-cooled CaO have been used to examine the higher vibrational levels of the $A'^1\Pi(X\sigma\pi^{-1})$ state (v=10-17) and the v=6-8 vibrational levels of the $C^1\Sigma^*(B\sigma\sigma^{-1})$ state. A perturbation of v=17 of the A' state was evident, caused by a spin-orbit mediated interaction with the $b^3\Sigma^*(\Omega=1)(X\sigma\sigma^{-1})$ v=14 level. Ro-vibrational constants for the A' state were obtained by fitting to the data for nominally unperturbed levels. The average radiative lifetime for the $A'^1\Pi(X\sigma\pi^{-1})$ state v=10-17 levels was 2.6 μ s, with no measurable dependence on v. This was consistent with the theoretical prediction of a relatively small transition dipole moment for the $A'^1\Pi-X^1\Sigma^*$ band system.

A homogeneous perturbation of the $C^1\Sigma^*(B\sigma\sigma^{-1})$ v = 7 level was examined by means of dispersed laser induced fluorescence (DLIF) and radiative lifetime measurements. The DLIF spectra clearly demonstrate that the perturbing $\Omega=0^+$ state is a component of a triplet state. Intense transitions from this state to the $a^3\Pi(0^+)(X\sigma\pi^{-1})$ state were observed. Configurational arguments are presented that support assignment of the perturbing state as the v = 12 vibrational level of the previously unobserved $g^3\Pi(0^+)(B\sigma\pi^{-1})$ state. © 2020 Elsevier Inc. All rights reserved.

1. Introduction

The electronic spectrum of the CaO molecule is complex due to the large number of low-energy electronic states and the many rovibronic interactions among them [1–13]. Field and co-workers have contributed many pioneering studies of CaO [4-14]. They developed an atomic-ions-in-molecule model and a configurational notation that greatly facilitates discussion of the electronic structure [6,8]. The ground state of CaO is $X^1\Sigma^+$, which is formally attributed to $Ca^{2+}(^{1}S_{0})O^{2-}(^{1}S_{0})$, a configuration that gives rise exclusively to one electronic state of ${}^{1}\Sigma^{+}$ symmetry. All of the lower energy excited electronic states are attributed to configurations of the Ca⁺ + O⁻ atomic-ion pair. These states can be mapped as combinations of molecular states from CaF [15] (which is a model for the electronic structure of the Ca⁺ ion in the axial field of the O⁻ ion) and NaO [16] (which is a model for the electronic structure of the O⁻ ion in the axial field of the Ca⁺ ion). The Ca⁺ $X\sigma$, $A\pi$, and $B\sigma$ orbitals correspond to the $X^2\Sigma^+$, $A^2\Pi$, and $B^2\Sigma^+$ states of CaF. For O⁻, the π^{-1} and σ^{-1} hole-orbitals correspond to the $X^2\Pi$ and $A^2\Sigma^+$ states of NaO. The various occupations of these atomic-ion orbitals combine to give the electronic configurations of the CaO molecule. For example, the Ca⁺(4s)O⁻($2p\sigma^22p\pi^3$) config-

E-mail address: mheaven@emory.edu (M.C. Heaven).

uration is specified as $X \sigma \pi^{-1}$ and gives rise to the molecular states $A'^1\Pi$ and $a^3\Pi_i$. A convenient table showing the lower energy configurations and their associated electronic states is given in reference [8].

High-level theoretical studies of CaO have been reported. mostly focused on the ground state and the group of low energy states arising from $X\sigma\pi^{-1}$ (A' $^{1}\Pi$ and $a^{3}\Pi_{i}$) and $X\sigma\sigma^{-1}$ (A $^{1}\Sigma^{+}$ and $b^3\Sigma^+$) [4,17–21] configurations. Khalil et al. [19,20] used highlevel multi-reference configuration interaction (MRCI) methods with basis sets of 5-zeta quality to predict the potential energy curves, dipole moments and electronic transition dipole moments for the X, A, A', a, and b states. The potential energy curves and wavefunctions from that work were used in subsequent calculations of the ro-vibronic eigenstates [19]. Spin-orbit and Luncoupling perturbations were included, producing results that could be compared directly with measured term energies. In 2016, Yurchenko et al. [22] refined the potential energy curves and perturbation matrix elements of Khalil et al. [19,20] by fitting to a very extensive set of experimentally determined term energies. Einstein A coefficients for spontaneous emission were also reported [22]. These data have been included in the ExoMol database [23], the use of which includes the identification of molecular species in the absorption and emission spectra of astrophysical objects. A pertinent example being the detection of CaO emission bands from the wake of a meteorite in 2018 [24].

^{*} Corresponding author.

A comprehensive summary of the experimental studies of the CaO spectrum was provided by Yurchenko et al. [22]. Here we mention selected studies that are of particular relevance to the present work. Data for the $A'^{1}\Pi(X\sigma\pi^{-1})$ state was obtained from emission spectra and deperturbation analyses. Field et al. [12] observed a vibrationally resolved $A'^1\Pi - X^1\Sigma^+$ chemiluminescence spectrum, and reported band heads that included the $A'^{1}\Pi(X\sigma\pi^{-1})$ vibrational levels from v = 9 to 21. Rotationally resolved A'-X emission bands, originating from the $A^{\prime 1}\Pi v = 0-3$ vibrational levels, were reported by Focsa et al. [25] Perturbations of the A' v = 2 and 3 levels were analyzed and attributed to interactions with the $b^3\Sigma^+(X\sigma\sigma^{-1})$ state. The $a^3\Pi(X\sigma\pi^{-1})$ state was observed as part of the "orange bands" of CaO. The $a^3\Pi(X\sigma\pi^{-1})$ v = 0 level was characterized through observations of the $c^3\Sigma^+(A\pi\pi^{-1})$ - $a^3\Pi$, $d^3\Delta(A\pi\pi^{-1})$ - $a^3\Pi$, and $e^{3}\Sigma^{-}(A\pi\pi^{-1})-a^{3}\Pi$ (0,0) bands [5,8,10,11]. Data for the vibrationally excited levels was derived from the $d^3\Delta(A\pi\pi^{-1})$ - $a^3\Pi$ $(X\sigma\pi^{-1})$ (1,1) and B¹ $\Pi(A\pi\sigma^{-1})$ -a³ $\Pi(0^{+})(X\sigma\pi^{-1})$ (3,0) bands, while perturbations, mostly resulting from interactions with the $A^1\Sigma^+$ state, yielded information for the v = 6, 9, and 12 levels of the $a^3\Pi(0^+)$ state. Perturbing interactions between $A^1\Sigma^+(X\sigma\sigma^{-1})$ and $A^{\prime 1}\Pi(X\sigma\pi^{-1})$ were also investigated by Field [13] and Focsa et al. [25] Spin-orbit perturbations between the A' $^{1}\Pi(X\sigma\pi^{-1})$ and b $^{3}\Sigma^{+}$ $(X\sigma\sigma^{-1})$ states have been observed. The A'¹ Π state is a pure Ω = 1 state with e- and f-symmetry components for every value of J. The spin-orbit interaction is homogeneous and follows the $\Delta\Omega$ = 0 selection rule. The $b^3\Sigma^+$ state has three spin-components, F_1 and F_3 are of f-symmetry and are approximately 50:50 mixtures of Ω = 0 and 1 whereas F_2 is of e-symmetry and of pure Ω = 1 character. Perturbations involving the F₁ and F₃ components of the b state will be observable in the Q branch of the A'-X transition and those involving the F2 component will be observable in the R and P branches of the A'-X transition.

Higher energy states have been investigated [1,2,7-9,26], including those that originate from the $A\pi\pi^{-1}$, $A\pi\sigma^{-1}$, $B\sigma\pi^{-1}$, and $B\sigma\sigma^{-1}$ configurations. Of significance for the present study, Stewart et al. [26] examined the laser induced fluorescence (LIF) spectrum of expansion-cooled CaO over the energy range 28.000-33,150 cm⁻¹. They observed progressions of the $C^1\Sigma^+(B\sigma\sigma^{-1})$ - $X^{1}\Sigma^{+}$ and $F^{1}\Pi(B\sigma\pi^{-1})-X^{1}\Sigma^{+}$ transitions that provided data for the higher vibrational levels of the excited states. Three vibrational bands of an unidentified $\Omega = 0^+ - X^1 \Sigma^+$ (v" = 0) transition were also observed. One of these vibronic states was found to be a perturber of the $C^1\Sigma^+(B\sigma\sigma^{-1})$ v = 7 level, pushing this state up in energy by approximately 7 cm⁻¹. In the following we designate this new state as y0⁺. Based on an extrapolation of the known vibrational levels of the $C^{1}\Sigma^{+}(A\pi\pi^{-1})$ state, Stewart et al. [26] speculated that the $y0^+-X^1\Sigma^+$ bands may be part of the $C'^1\Sigma^+-X^1\Sigma^+$ system. However, based on spin-orbit selection rules for perturbations mediated by a one-electron operator (e.g., spin-orbit and L-uncoupling interactions), Field [27] argued that the matrix elements between the $C^1\Sigma^+(B\sigma\sigma^{-1})$ and $C'^1\Sigma^+(A\pi\pi^{-1})$ states would be small. He suggested that the $g^3\Pi(0^+)(B\sigma\pi^{-1})$ or $f^3\Pi(0^+)(A\pi\sigma^{-1})$ states were viable candidates for interactions with the $C^1\Sigma^+(B\sigma\sigma^{-1})$ state, and that the triplet character of the perturbing state could be established by observing the dispersed fluorescence spectrum.

There were two main motives for our reexamination of the spectrum of expansion-cooled CaO. The red spectral range (13,700–17,150 cm $^{-1}$) was covered as part of our search for bands of the hypermetallic oxide CaOCa [28,29]. Bands of CaO were present under all of the conditions used for this survey, and rotationally resolved data were obtained for the $A'^1\Pi$ ($X\sigma\pi^{-1}$)- $X^1\Sigma^+$ transition for upper state vibrational levels spanning the range v = 10–17. The second objective was to probe the identity of the state that perturbs the $C^1\Sigma^+(B\sigma\sigma^{-1})$ state near v = 7 by means of wavelength- and time-resolved fluorescence measurements.

2. Experimental

Fig. 1 shows the instruments used to record LIF and dispersed laser induced fluorescence (DLIF) spectra of CaO. To produce the oxide, 1064 nm light from a pulsed Nd/YAG laser (Quanta-Ray, DCR 1A) was focused onto a Ca rod target (ESPI Metals, 99.9% pure) using a 30 cm focal length lens. The plane polarized output from the Nd/YAG laser was attenuated to the 1-10 mJ/pulse range by means of a Glan-Taylor prism housed in a rotatable stage (Thorlabs CCM1-PBS25-1064-HP/M). The Ca rod was rotated and translated continuously to ensure a fresh metal surface for each ablation pulse. The calcium vapor was entrained in a gas mixture consisting of He and O₂ in a 9:1 volume ratio. The operating pressure behind the valve was 15 atm. Gas pulses were generated by a Parker-Hannifin General Valve (Series 9) with a pulse duration of 1 ms. The entrained metal vapor-gas mixture was supersonically expanded through a 2 mm diameter orifice into a vacuum chamber. The vacuum was maintained by a Roots blower (Leybold, RUVAC WSU 251) backed by a rotary vane pump (Leybold, TRIVAC D65B). The average background pressure in the chamber was typically less than 100 mtorr under gas loading, such that a Campargue expansion was formed.

Molecules present in the supersonic expansion were probed with a pulsed tunable dye laser (Lambda-Physik, FL3002e), pumped by a XeCl excimer (Lambda-Physik, Compex Pro 201), with a pulse repetition frequency of 10 Hz, nominal pulse duration of 10 ns and linewidth (FWHM) of 0.3 cm⁻¹. For the recording of rotationally resolved data, the linewidth was reduced to 0.06 cm⁻¹ by adding an intracavity etalon. The absolute wavenumber calibration was established by directing a fraction of the dye laser light through a cell of iodine vapor for simultaneous recording of the I₂ *B-X* excitation spectrum (LIF detected by a Hamamatsu R955 photomultiplier). Resultant spectra were fitted to the I₂ spectral transition energies of Salami and Ross [30]. To access states of CaO in the near uv spectral range, the output from the dye laser

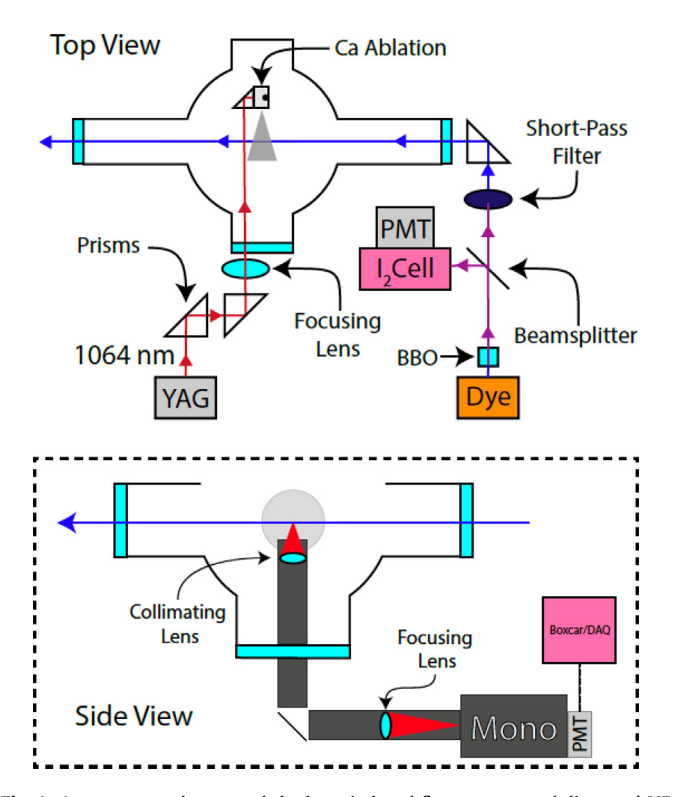


Fig. 1. Apparatus used to record the laser induced fluorescence and dispersed LIF spectra of CaO. For excitation in the visible range, the BBO crystal and the short-pass filter were removed.

was frequency doubled by an angle-tuned BBO crystal (Lambda Physik, FL30) while the wavenumber calibration was obtained by using the dye laser fundamental to record the I₂ spectrum.

The laser light was directed into the vacuum chamber, perpendicular to the supersonic expansion, ~ 3 cm downstream from the pulsed expansion nozzle. A two-lens telescope consisting of a collimating lens (Thorlabs, focal length f = 6 cm, diameter D = 5.1 cm) and an achromatic focusing lens (Thorlabs, f = 25 cm D = 5.1 cm) collected light orthogonal to both the jet expansion axis and the probe laser beam axis. Two 4-channel digital delay generators (DDG) were used to control the timings between the ablation and probe lasers, as well as the data collecting equipment (Quantum Composers Model 9614 and Stanford Research Systems DG535).

For LIF measurements, a PMT (Hamamatsu R955) with a longpass filter, typically with a 50% transmission edge at a wavelength ~50 nm longer than that of the laser, was placed near the imaging focal point of the lens system. The signal from the PMT was sent to both an oscilloscope (Tektronix TDS 2014) and a pair of time-gated boxcar integrators (Stanford Research Systems, SRS 250). The background signal was subtracted from the fluorescence signal and averaged using an analog signal processor (Stanford Research Systems, SRS 235). A combination digital/analog input/output data acquisition device (DAQ) (National Instruments, USB-6210) was used to collect the 30-shot averaged data for each laser wavelength, and the laser wavelength was advanced in 0.003 nm increments using the same DAQ. A LabVIEW 2018 (National Instruments) routine managed the incoming and outgoing signals. The uncalibrated wavelength from the laser diffraction grating sine drive, CaO fluorescence signals and I2 reference data were stored for later calibration and interpretation. Time-dependent fluorescence decay curves for selected rovibronic levels were collected by averaging the oscilloscope traces from 128 laser pulses.

For the DLIF experiments, the emitted light was directed into a monochromator (Instruments SA, 0.64 m, f/5.8, 1200 grooves/mm diffraction grating) and then to either an intensified charge-coupled device camera (iCCD) (Andor iStar USB) or the PMT. A custom C program was developed, housed on an embedded system (Arduino Mega 2650), to drive two stepper-motor controller units, one of which controls a stepper-motor connected to the sine drive of the monochromator diffraction grating, and the other was used to raise or lower a mirror that diverted the dispersed light to either the PMT or iCCD to obtain temporal or broadband spectroscopic information, respectively. The camera was controlled and data collected using the Solis (Andor) software.

3. Results

(i). The A' $^{1}\Pi$ (X $\sigma\pi^{-1}$)-X $^{1}\Sigma^{+}$ bands

LIF spectra recorded in the 13,700-17,150 cm⁻¹ range were dominated by the $A^1\Sigma^+(X\sigma\sigma^{-1})-X^1\Sigma^+$ and $A'^1\Pi(X\sigma\pi^{-1})-X^1\Sigma^+$ bands. The latter were easily distinguished from the A-X bands as they exhibited Q-branches in the rotationally resolved scans, and much longer fluorescence decay lifetimes. Fig. 2 shows the rotational structure of the A'-X (10,0) band, along with a simulation generated by means of the PGOPHER software [31]. Fitting of the A' state band origins and rotational constants was carried out using PGOPHER. The A'-X bands have a combination difference-defect between the Q-lines and the P/R-lines because these transitions sample respectively f-symmetry and esymmetry lambda-doublet components [25]. However, this combination defect was below the precision of the present measurements and the bands were fitted with the lambda-doubling parameters set to zero. The relatively cold rotational population distributions (T_{Rot} < 100 K) limited the range of rotational levels

observed, such that the fitted centrifugal distortion constants were not statistically significant when treated as adjustable parameters. The theoretical calculations of Yurchenko et al. [22] provide some indication of the magnitudes of the neglected terms. Examination of the A' $\Pi(X\sigma\pi^{-1})$ energy levels from the Exomol database indicates that the lambda doublet splitting for v = 10 increases from 5×10^{-4} cm⁻¹ for rotational level J = 1 to 0.08 cm⁻¹ at J = 25(the range of J typically observed in the spectra). Fitting to the mean energies of the -e and -f parity levels yields a centrifugal distortion constant of 4.4×10^{-7} cm⁻¹, in reasonable agreement with the prediction from the Kratzer relationship of $D_e = 5.5 \times 10^{-7}$ cm⁻¹. As we did not have sufficient resolution to determine the lambda doublet splittings and distortion constants, and did not have a reliable way to predict these values due to the presence of perturbations, they were set to zero in the fits to the rotational line positions. Hence, only the band origins and upper state rotational constants were varied in the spectral fitting. The resulting effective molecular constants are listed in Table 1. The rotational line positions for all A'-X bands observed in the present study have been provided as Electronic Supplementary Information.

Fluorescence decay lifetimes were recorded for all rotationally resolved A'-X bands. In a series of test experiments, we found that the lifetimes did not exhibit any significant variation with the rotational level. Consequently, the lifetime data reported here were obtained from measurements made using excitation of the most intense rotational line of a given band. Each fluorescence decay curve was well-represented by a single exponential function, and the fitted lifetimes are listed in Table 2. Non-linear least squares fitting was carried out using the program Origin Pro 8.5.1.

(ii). Wavelength- and time-resolved fluorescence measurements for the $C^1\Sigma^*(B\sigma\sigma^{-1})$ and $y0^*$ states.

Stewart et al. [26] observed transitions to the y0⁺ state at 32037.0, 32479.5 and 32955.2 cm^{-1} , and these upper states were labeled as the vibrational levels n-1, n and n+1. The $y0^+$ n state interacts strongly with $C^1\Sigma^+(B\sigma\sigma^{-1})$ v = 7, while v0⁺ n-1 and n+1lie above and below C v = 6 and v = 8, respectively. This smaller vibrational spacing of the $y0^+$ state relative to that of the $C^1\Sigma^+$ (- $B\sigma\sigma^{-1}$) state implies that the y0⁺ state belongs to a π^{-1} configuration. To facilitate configurational assignment of the y0⁺ state we recorded DLIF spectra for excitation to each of the y0+ vibronic levels and to the $C^1\Sigma^+(B\sigma\sigma^{-1})$ v = 6, 7, and 8 levels. These data are presented in Fig. 3, where the energy scale gives the energy of the lower vibronic state of the observed transition relative to $X^{1}\Sigma^{+}$ v = 0. The bands in these traces were readily assigned using term energies from the literature. All of the fluorescence transitions to states that lie below 12,000 cm⁻¹ terminate on the vibrational levels of the $X^1\Sigma^+$ state. The bands observed in the 12,000– 16,000 cm⁻¹ range terminate on A¹ Σ ⁺($X\sigma\sigma^{-1}$) v = 1–5 and a³ $\Pi(0^+)$ $(X\sigma\pi^{-1})$ v = 10–12. Fluorescence decay lifetimes were measured for the six upper states and these are collected in Table 3. Decay curves were obtained with the laser tuned to the band head for each vibronic transition, corresponding to an upper state rotational quantum number of approximately J = 4.

4. Analysis and discussion

The band origin data for the $A'^1\Pi(X\sigma\pi^{-1})$ state are compared to the results from the experimental study of Field et al. [12] and the line list data of ExoMol [22] in Table 1, where we present the differences between the literature values and the present determinations. Field et al. [12] reported band head data for the red-shaded emission bands, so it was expected that the heads would lie approximately 2 cm⁻¹ higher in energy than the origins. There is

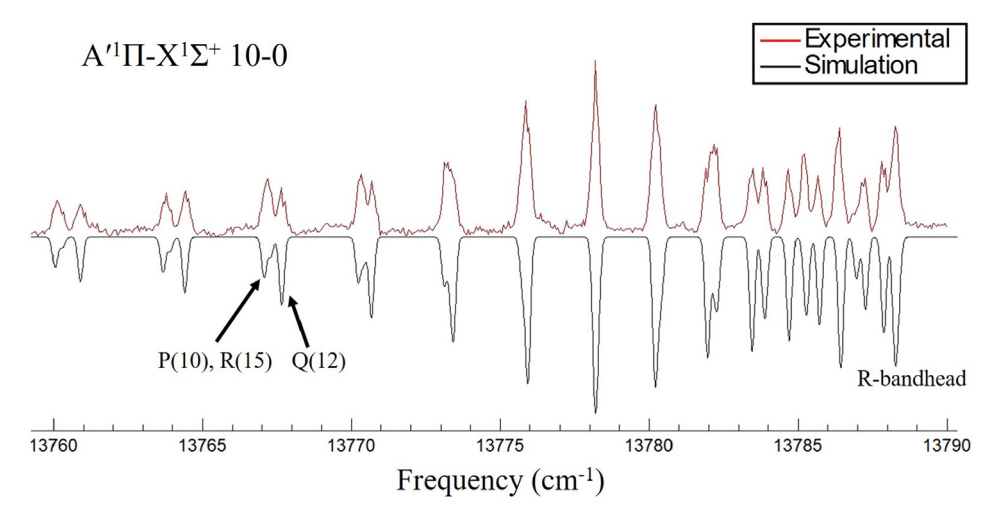


Fig. 2. LIF spectrum of the CaO $\Lambda'^1\Pi(X\sigma\pi^{-1})-X^1\Sigma^+$ (10,0) band. The downward-going trace is a simulation generated using the program PGOPHER.

Table 1 Molecular constants for the $A'^1\Pi(X\sigma\pi^{-1})$ state.

v	$\begin{array}{c} B_{\nu} \\ (cm^{-1})^a \end{array}$	$\begin{array}{l} T_{\nu,0} \\ (cm^{-1})^b \end{array}$	δE, Ref. [12]	δE, Ref. [22]	Number of lines fit	in
10	0.3175	13787.23	2.8	-0.8	38	
11	0.3148	14276.94	3.1	-1.1	63	
12	0.3121	14761.41	1.6	-1.7	60	
13	0.3101	15240.50	2.5	-2.1	52	
14	0.3074	15714.72	0.3	-2.8	64	
15	0.3039	16184.08	2.5	-3.5	26	
16	0.3014	16648.80	5.2	-4.5	20	
17	0.3016	17108.85	4.2	-10.7	24	
$T_{0,0}$					8608.1(2)
ω_{e}					546.2(1)	
$\omega_{e}x_{e}$	2				2.57(1)	
B_e					0.3440(1	5)
α					0.00255(11

 $^{^{\}rm a}1 - \sigma \ {\rm error} \pm 0.0005 \ {\rm cm}^{-1}.$

Table 2 Fluorescence decay lifetimes for the $A'^1\Pi(X\sigma\pi'^{-1})$ state.

Vibrational level	$\tau/\mu s^a$
10	2.4
11	2.7
12	2.6
13	2.5
14	2.6
15	2.8
16	2.9
17	2.7

 $^{^{}a}$ ±0.2 μ s, with the inclusion of experimental errors.

a significant deviation for the v=17 level, but it is apparent from both the rotational constant and the term energy that this level is perturbed in the ExoMol model [22]. The last column in Table 1 is the difference between the R(0) transition energies obtained from the ExoMol line list [22] and the measured values. The difference increases with increasing v, suggesting that the perturbation model requires further refinement. We also compared rotational constants derived from the ExoMol [22] data to the measured values. For this purpose, we generated rotational constants from ExoMol by fitting the rotational energies to the rigid rotor expression $E_v(J) = B_vJ(J+1)$ for the range of rotational levels sampled by the

jet-cooled spectra (J = 1–25). With the exception of B₁₆ and B₁₇ (predicted values of 0.3026 and 0.3062 cm⁻¹ and observed values of 0.3014 and 0.3016 cm⁻¹), the ExoMol rotational constants were within the experimental uncertainties of the constants given in Table 1.

Ro-vibrational constants for the $A'^1\Pi(X\sigma\pi^{-1})$ state were determined by fitting to the energy levels that appeared to be relatively unperturbed. We have used the v=0 and 1 term energies provided by Focsa et al. [25] and the v=10–15 data from the present measurements. The vibrational term energies were fit to the expression

$$T_{v,0} = T_{0,0} + \omega_e v - \omega_e x_e v(v+1)$$
 (1)

The standard deviation of the fit was 0.23 cm $^{-1}$, and the constants are listed in Table 1. Trial fits that included the $\omega_e y_e$ anharmonicity constant did not yield statistically significant results for this parameter. Rotational constants for this same set of vibrational levels were fit by the expression

$$B_v = B_e - \alpha_e(v + 1/2) \tag{2}$$

and the resulting constants are given in Table 1. The standard deviation for this fit was 0.0007 cm $^{-1}$ (this was the standard deviation of $B_{\nu}(\text{obs})$ - $B_{\nu}(\text{fit})$).

We examined the energy level predictions from the ExoMol [22] model to identify the state that would be the most probable cause of the perturbation of the $A'^1\Pi(X\sigma\pi^{-1})$ v = 17 state. It was immediately apparent that the calculated energies for the $A^{\prime 1}\Pi(X\sigma\pi^{-1})$ $v = 17 (17098.7 \text{ cm}^{-1}) \text{ and } b^3 \Sigma^+ (X \sigma \sigma^{-1}) v = 14 (17109.9 \text{ cm}^{-1})$ states were close enough for a significant interaction. These states can be coupled by the one-electron spin-orbit operator to give matrix elements of the form [13,25] $H_{SO} = a_{\pi} \langle A', v'|b, v \rangle / \sqrt{2}$, where the term in bra-ket notation is the vibrational wavefunction overlap integral, and a_{π} is the spin-orbit coupling constant for O (approximately-121 cm⁻¹) [13]. A quantitative test of this model was made using Morse potential energy curves (MPEC) for the $A'^{1}\Pi(X\sigma\pi^{-1})$ and $b^{3}\Sigma^{+}(X\sigma\sigma^{-1})$ states, in order to generate vibrational wavefunctions and overlap integrals. The MPEC for the $A'^{1}\Pi(X\sigma\pi^{-1})$ state was determined using the molecular constants given in Table 1. The MPEC for the $b^3\Sigma^+(X\sigma\sigma^{-1})$ state was more difficult to assess due to the lack of spectroscopic data (only the v = 1level has been observed [14]). As a starting point we used the theoretically predicted of constants [20] T_0 = 9282, ω_e = 585.7 and ω_e $x_e = 3.16 \text{ cm}^{-1}$, with an equilibrium distance of $R_e = 1.96 \text{ Å}$. The energy levels generated from these parameters were compared to the experimentally determined term energy for $b^3\Sigma^+(X\sigma\sigma^{-1})$ v = 1 of 10073.3 cm⁻¹ [14], and the predictions from ExoMol.

 $^{^{\}rm b}1 - \sigma \ {\rm error} \pm 0.05 \ {\rm cm}^{-1}$

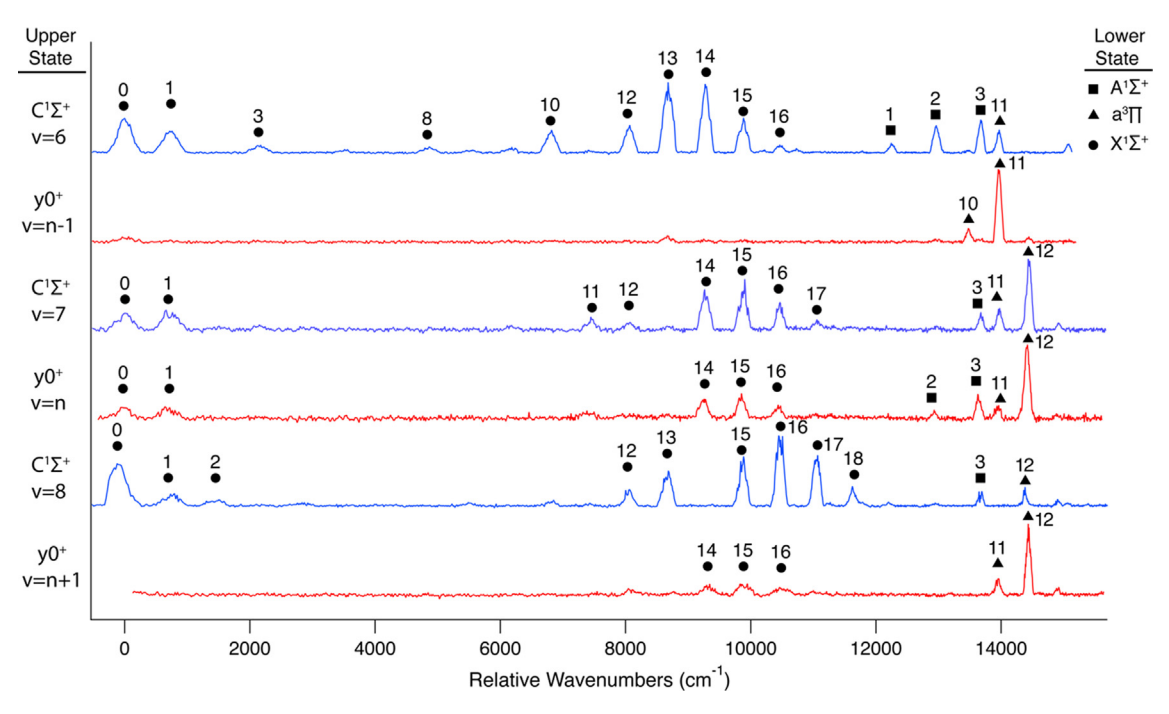


Fig. 3. Dispersed LIF spectra for CaO using excitation of the states $C^1\Sigma^+(B\sigma\sigma^{-1})$ v=6,7, and 8, and $y0^+v=n-1,n$ and n+1. The filled symbols indicate the lower electronic state, with $\bullet=X^1\Sigma^+$, $\blacksquare=A^1\Sigma^+(X\sigma\sigma^{-1})$, and $\triangle=A^3\Pi(0^+)(X\sigma\pi^{-1})$.

Table 3 Fluorescence decay lifetimes for the $C^1\Sigma^*(B\sigma\sigma'^{-1})$ and $y0^*$ states.

State	τ/ns ^a	
C v = 6	29	
C v = 7	32	
C v = 8	24	
$y0^{+} n - 1$	46	
y0 ⁺ n	35	
$y0^{+} n + 1$	42	

 $^{\rm a}$ ±5 ns, with the inclusion of experimental errors.

The above molecular constants underestimated the known energy of the $b^3\Sigma^+(X\sigma\sigma^{-1})$ v = 1 level and the ExoMol prediction that the $b^3\Sigma^+(X\sigma\sigma^{-1})$ v = 14 level is just above A' $^1\Pi(X\sigma\pi^{-1})$, v = 17. Consequently, we adjusted the T_0 , ω_e and $\omega_e x_e$ values for $b^3 \Sigma^+ (X \sigma \sigma^{-1})$ to produce this latter condition, while also imposing the restriction that the fitted molecular constants recovered the experimentally determined term energy for $b^3 \Sigma^+ (X \sigma \sigma^{-1}) v = 1$. The constants T_0 = 9489, ω_e = 590.4, $\omega_e x_e$ = 3 cm⁻¹ satisfied these conditions. The A' $^{1}\Pi(X\sigma\pi^{-1})$ -b $^{3}\Sigma^{+}(X\sigma\sigma^{-1})$ Franck-Condon factors were then calculated using the program Level 8.0 [32], and the unsigned overlap integrals were obtained as the square roots of the Franck-Condon factors. This procedure yielded $|\langle v' = 17 | v = 14 \rangle| = 0.054$ and a spin-orbit matrix element of $|H_{SO}| = 4.6 \text{ cm}^{-1}$. Unperturbed rotational constants were predicted to be $B_{17} = 0.300 \text{ cm}^{-1}$ for $A'^{1}\Pi(X\sigma\pi^{-1})$ and $B_{14} = 0.344$ cm⁻¹ for $b^{3}\Sigma^{+}(X\sigma\sigma^{-1})$. With an energy gap of 12 cm⁻¹ between the J = 0 levels of the unperturbed $A'^{1}\Pi$ $(X\sigma\pi^{-1})$ v = 17 and b³ $\Sigma^+(X\sigma\sigma^{-1})$ v = 14 states, a two-state perturbation model recovered the experimental value for the effective rotational constant for low rotational levels of $A^{\prime 1}\Pi(X\sigma\pi^{-1})$ v = 17. The model indicated that the band origin had been pushed down by 1.6 cm⁻¹. As part of this exercise, we also examined the $A'^{1}\Pi(X\sigma\pi^{-1})$ v = 16/ $b^{3}\Sigma^{+}(X\sigma\sigma^{-1})$ v = 13 pair to assess the degree to which they interact. In this case the $b^3\Sigma^+(X\sigma\sigma^{-1})$ v = 13 state is estimated to lie $30~\rm cm^{-1}$ below $A'^1\Pi(X\sigma\pi^{-1})$ v = 16. Due to this larger energy gap, and the small overlap integral $(|\langle v'=16|v=13\rangle|=0.0046)$, we found this interaction to be unimportant for the resolution of the present experiments. Overall, this analysis supports the assignment of the $A'^1\Pi(X\sigma\pi^{-1})$ v = 17 state perturbation to the interaction with $b^3\Sigma^+(X\sigma\sigma^{-1})$ v = 14.

Fluorescence decay lifetimes for the $A'^1\Pi(X\sigma\pi^{-1})$ state were found to be almost independent of the vibrational level over the range v=10–17. Field [13] had noted that the $A'^1\Pi(X\sigma\pi^{-1})$ - $X^1\Sigma^+$ transition dipole moment would be small, resulting in spontaneous decay lifetimes on the order of 10 μ s. The observed values are somewhat shorter, but consistent with the argument presented in Ref. [13]. As the ExoMol database [22] also includes the Einstein A coefficients, it was possible to generate theoretical values for the lifetime of the $A'^1\Pi(X\sigma\pi^{-1})$ state by summing the A coefficients over all final states. This yielded lifetimes that decreased from 11.4 μ s for v=10 down to 8.5 μ s for v=15. The predicted lifetime for v=17 was anomalous, being 15.4 μ s. This suggests that the calculated Einstein A coefficients for A'v=17 have been decreased by the effects of mixing with a long-lived state (a prediction that is not supported by the present lifetime measurements).

DLIF and lifetime measurements for the $C^1\Sigma^+(B\sigma\sigma^{-1})$ and $v0^+$ states provide useful insights for establishing the configurational parentage of the y0⁺ state. We begin by considering the DLIF spectra for the $C^1\Sigma^+(B\sigma\sigma^{-1})$ v = 6 and y0⁺ n-1 levels. The energy separation between these levels is large enough (59.4 cm⁻¹) that mixing between them is expected to be weak. The relevant traces in Fig. 3 show that $C^1\Sigma^+(B\sigma\sigma^{-1})$ v = 6 radiates back to both the $X^{1}\Sigma^{+}$ and $A^{1}\Sigma^{+}$ ($X\sigma\sigma^{-1}$) states, as expected. A transition to $a^{3}\Pi$ $(0^+)(X\sigma\pi^{-1})$ v = 11 is also present. This is probably mediated by the mixing of this lower level with nearby levels of the $X^1\Sigma^+$ and $A^{1}\Sigma^{+}(X\sigma\sigma^{-1})$ states (see Fig. 7 of reference [19]). In contrast, the DLIF spectrum obtained using excitation of $y0^+ n - 1$ is dominated by transitions to the $a^3\Pi(0^+)(X\sigma\pi^{-1})$ state v = 10 and 11 level. The transitions to singlet lower states are barely discernable above the noise level. This clearly indicates that the y0⁺ state is a triplet state. Furthermore, the short radiative lifetime of $y0^+ n - 1$ indicates that the y0⁺-a³ $\Pi(0^+)(X\sigma\pi^{-1})$ transition has a large transition dipole

moment. Similar trends are evident for the $C^1\Sigma^+(B\sigma\sigma^{-1})$ v = $8/y0^+$ n+1 pair of states, which are separated by 52.3 cm⁻¹. The emission from $y0^+$ n+1 is dominated by the triplet bands, but, as compared to the spectrum from the n-1 level, the singlet bands are somewhat stronger. This suggests that the n+1 state has a small fractional singlet character. The emission from the $C^1\Sigma^+(B\sigma\sigma^{-1})$ v = 8 level was dominated by transitions to singlet final states.

Next, we consider the $C^1\Sigma^+(B\sigma\sigma^{-1})$ v = 7 / y0⁺ n pair of states. The perturbation analysis presented in Ref. [26] concluded that these states were separated by 9.4 cm⁻¹ prior to their mutual repulsion. The eigenvectors from the deperturbation analysis indicated a nearly 50:50 mixing of the two states. This prediction was borne out by the DLIF spectra that show both singlet and triplet bands with comparable intensities. Note also that the lifetime behavior is consistent. The results for $C^1\Sigma^+(B\sigma\sigma^{-1})$ v = 6 and 8 give an average lifetime of 27 ns, and those for y0⁺ n – 1 and n + 1 give a lifetime of 44 ns. Hence a 50:50 mixed state, in the absence of interference effects , should exhibit a lifetime of 33 ns (based on the weighted sum of decay rates). This is the average of the values observed for $C^1\Sigma^+(B\sigma\sigma^{-1})$ v = 7 and y0⁺ n.

Having established that the y0⁺ state derives from a triplet state, the next step was to determine the identity of the state. This process was guided by the observations that $y0^+$ perturbs $C^1\Sigma^+$ $(B\sigma\sigma^{-1})$ and radiates to $a^3\Pi(0^+)(X\sigma\pi^{-1})$. Viable candidates for the perturbing state are $g^3\Pi(0^+)(B\sigma\pi^{-1})$ and $f^3\Pi(0^+)(A\pi\sigma^{-1})$. Of these two, $g^3\Pi(0^+)(B\sigma\pi^{-1})$ can radiate to $a^3\Pi(0^+)(X\sigma\pi^{-1})$ via a oneelectron process while the transition from $f^3\Pi(0^+)(A\pi\sigma^{-1})$ would require a two-electron process. Based on these considerations, and the indication from the vibrational intervals that y0⁺ is derived from a π^{-1} configuration, we recommend the assignment of the $y0^+$ state as $g^3\Pi(0^+)(B\sigma\pi^{-1})$. Finally, we speculate on the vibrational numbering for the observed levels of the $g^3\Pi(0^+)$ ($B\sigma\pi^{-1}$) state. This state has not been characterized previously, but the term energy of the v = 0 level can be estimated by considering the singlet-triplet energy splittings associated with the π^{-1} states. The $B\sigma\pi^{-1}$ configuration also gives rise to the F¹ Π state, for which the term energy and vibrational constants have been determined $(T_{00} = 26794.5, \omega_e = 521.3, \omega_e x_e = 2.59 \text{ cm}^{-1})$ [26]. Representative isoconfigurational singlet-triplet energy splittings are provided by $\Delta E(A'^{1}\Pi - a^{3}\Pi(1), X\sigma\pi^{-1}) = 257 \text{ cm}^{-1}, \Delta E(D^{1}\Delta - d^{3}\Delta(2), A\pi\pi^{-1}) =$ -210 cm^{-1} , and $\Delta E(E^{1}\Sigma^{-}-e^{3}\Sigma^{-}, A\pi\pi^{-1}) = -53 \text{ cm}^{-1}$ [8]. If we assume that the vibrational constants are the same for the $g^3\Pi$ $(0^+)(B\sigma\pi^{-1})$ and $F^1\Pi(B\sigma\pi^{-1})$ states, we can use the vibrational interval between the v = n + 1 and v = n - 1 states to obtain the energy of the n = 12 level. Extrapolation to v = 0 then yields a term energy for the $g^3\Pi(0^+)(B\sigma\pi^{-1})$ state of $T_{00} = 26,644$ cm⁻¹, and a singlet-triplet energy splitting of $\Delta E(F^1\Pi - g^3\Pi(0^+), B\sigma\pi^{-1}) = 151$ cm^{-1} . The vibrational numberings n = 11 and n = 13 would yield unlikely values for $\Delta E(F^1\Pi - g^3\Pi(0^+))$. Overall, this analysis shows that the assignment of y0⁺ as the $g^3\Pi(0^+)(B\sigma\pi^{-1})$ state is entirely consistent with the atomic-ions-in-molecule model for CaO.

CRediT authorship contribution statement

Sean M. Bresler: Investigation, Formal analysis, Visualization, Methodology, Writing - original draft. **Joel R. Schmitz:** Investiga-

tion, Formal analysis, Visualization, Methodology. **Michael C. Heaven:** Conceptualization, Writing - original draft. **Robert W. Field:** Conceptualization, Formal analysis, Writing - original draft.

Declaration of Competing Interest

The authors declared that there is no conflict of interest.

Acknowledgement

This material is based upon work supported by the National Science Foundation under 1946950. RWF thanks the NSF (CHE-1800410) for support of his part of this collaboration.

Appendix A. Supplementary material

Supplementary data to this article can be found online at https://doi.org/10.1016/j.jms.2020.111293.

References

- [1] A. Lagerqvist, Arkiv. Fysik 8 (1954) 83-95.
- [2] A. Lagerqvist, Naturwissenschaften 40 (1953) 268-269.
- [3] M. Hultin, A. Lagerqvist, Ark. Fys. 2 (1951) 471-505.
- [4] J.F. Harrison, R.W. Field, C.C. Jarrold, ACS Symp. Ser. 828 (2002) 238–259.
- [5] D.P. Baldwin, J.B. Norman, R.A. Soltz, A. Sur, R.W. Field, J. Mol. Spectrosc. 139 (1990) 39–67.
- [6] D.P. Baldwin, E.J. Hill, R.W. Field, J. Am. Chem. Soc. 112 (1990) 9156–9161.
- [7] D.P. Baldwin, R.W. Field, J. Mol. Spectrosc. 139 (1990) 68-76.
- [8] J.B. Norman, K.J. Cross, H.S. Schweda, M. Polak, R.W. Field, Mol. Phys. 66 (1989) 235–268.
- [9] D.P. Baldwin, R.W. Field, J. Mol. Spectrosc. 133 (1989) 90-95.
- [10] R.F. Marks, H.S. Schweda, R.A. Gottscho, R.W. Field, J. Chem. Phys. 76 (1982) 4689–4691.
- [11] R.F. Marks, R.A. Gottscho, R.W. Field, Phys. Scr. 25 (1982) 312–328.
- [12] R.W. Field, G.A. Capelle, C.R. Jones, J. Mol. Spectrosc. 54 (1975) 156–159.
- [13] R.W. Field, J. Chem. Phys. 60 (1974) 2400–2413.
- [14] D.P. Baldwin, R.W. Field, J. Mol. Spectrosc. 139 (1990) 77–83.
- [15] S.F. Rice, H. Martin, R.W. Field, J. Chem. Phys. 82 (1985) 5023-5034.
- [16] J.N. Allison, R.J. Cave, W.A. Goddard III, J. Phys. Chem. 88 (1984) 1262–1268.
- [17] C.W. Bauschlicher Jr., D.R. Yarkony, J. Chem. Phys. 68 (1978) 3990–3997.
- [18] R.N. Diffenderfer, D.R. Yarkony, J. Chem. Phys. 77 (1982) 5573–5580. [19] H. Khalil, F. Le Quere, V. Brites, C. Leonard, J. Mol. Spectrosc. 271 (2012) 1–9.
- [20] H. Khalil, V. Brites, F. Le Quere, C. Leonard, Chem. Phys. 386 (2011) 50-55.
- [21] J. Cheng, H. Chen, X. Zhu, X. Cheng, J. Mol. Struct. 1084 (2015) 122–127.
- [22] S.N. Yurchenko, A. Blissett, U. Asari, M. Vasilios, C. Hill, J. Tennyson, Mon. Not. R. Astron. Soc. 456 (2016) 4524–4532.
- [23] J. Tennyson, S.N. Yurchenko, Mon. Not. R. Astron. Soc. 425 (2012) 21-33.
- [24] A.A. Berezhnoy, J. Borovicka, J. Santos, J.F. Rivas-Silva, L. Sandoval, A.V. Stolyarov, A. Palma, Planet. Space Sci. 151 (2018) 27–32.
- [25] C. Focsa, A. Poclet, B. Pinchemel, R.J. Le Roy, P.F. Bernath, J. Mol. Spectrosc. 203 (2000) 330–338.
- [26] J.T. Stewart, M.N. Sullivan, M.C. Heaven, J. Mol. Spectrosc. 322 (2016) 18-21.
- [27] R.W. Field, Discussion of CaO perturbations, 2016.
- [28] B. Ostojic, P. Jensen, P. Schwerdtfeger, P.R. Bunker, J. Mol. Spectrosc. 301 (2014)
- [29] B. Ostojic, P.R. Bunker, P. Schwerdtfeger, A. Gertych, P. Jensen, J. Mol. Struct. 1023 (2012) 101–107.
- [30] H. Salami, A.J. Ross, J. Mol. Spectrosc. 233 (2005) 157–159.
- [31] C.M. Western, J. Quant. Spectrosc. Radiat. Transfer 186 (2017) 221-242.
- [32] R.J. Le Roy, J. Quant. Spectrosc. Radiat. Transfer 186 (2017) 167–178.